J. Fluid Mech. (1971), *vol.* 47, *part* 1, *pp.* 145–170
Printed in Great Britain

A model of the mature hurricane

By G. F. CARRIER, A. L. HAMMOND AND O. D. GEORGE
Harvard University

(Received 24 July 1970)

A schematic picture of the structure of a mature hurricane is hypothesized. The heat and moisture transfer, the boundary-layer dynamics and the overall dynamic and thermodynamic balances are analysed crudely, but sufficiently accurately to provide support for the hypothesis.

1. Introduction

The mature tropical hurricane is the largest example of a class of intense swirling motions which occur naturally in the atmosphere. The structure of these flows, other instances of which include tornados, water spouts, fire storms and dust devils, seems not to have been fully explained as yet. Although the role of friction in assisting the growth of the storm by increasing the supply of fuel has been recognized (Charney & Eliassen 1964), the emphasis of much previous work on the hurricane has been on finding a parameterization of cumulus convection which would permit realistic life-cycles for model storms without clearly specifying the structure and the relevant physics involved (Ooyama 1969; Yamasaki 1968; and Rosenberg 1969). The need for very high moisture and heat content of the boundary-layer air also has long been recognized (Malkus & Riehl 1960). Nevertheless, no really consistent picture of the dynamics or energetics of the mature storm has appeared. The role of the frictionally-driven recirculation in the eye in maintaining the intense storm and the consequent implication that the energetics of the storm are secondary to the dynamics seems not to have been seriously considered. A model consistent with these ideas is proposed in this paper where, in § 3, we develop the analysis of the boundary-layer dynamics appropriate to the storm. In § 4 we estimate the maximum velocities which are to be expected from the structure proposed here and from the relevant thermodynamic information. In § 5 we ask whether there exists a family of circumferential velocity distributions for which the resulting boundary-layer flows have the required properties and we present results of numerical calculations for the flows. In § 6 we estimate the effect of the boundary-layer flows on the heat and moisture content of the atmosphere and on the flux of these quantities at the sea surface.

Before proceeding to a description of the model, however, it is useful to summarize some pertinent facts about these storms. Hurricanes (or typhoons) are large cyclonic storms which occur in all months of the year but most frequently in the late summer and early autumn months. They become fully developed over the oceans in tropical latitudes, usually below 20°, and many of them

eventually migrate towards higher latitudes; they do not occur within 5° of the equator. The area over which the organized motion occurs is of the order of 1000 miles or more in diameter, while the depth of the atmosphere which is significantly involved in the motion is only the lowest few miles.

Almost all observers are agreed as to the general characteristics of the storm. It is described as a roughly circular cyclonic vortex with low level inflow to and high level outflow from an annular region of intense rainfall, maximum winds, and strong updrafts. In the centre is a warm, dry, relatively quiescent core or 'eye'. Slow settling occurs in the core and in the outer region of the vortex; also in the outer regions, the high level outflow becomes anti-cyclonic. The release of latent heat energy by condensation of water vapour in the inner rain area provides the density distribution which is needed to maintain the pressure gradient which, in turn, is needed to balance the centripetal accelerations which characterize the storm. Extreme low central pressure (typically 960 m or below), high central temperature at upper levels (15 °C above ambient), high vortex winds (100–200 knots), and the presence of an eye distinguish the mature hurricane from the ordinary tropical depression, although by convention any tropical storm with winds exceeding 76 knots is so named.

2. Model hurricane structure

The foregoing facts seem to be consistent with the idealized structure shown schematically in figure 1. It consists of four dynamically distinct regions, which may be qualitatively described as follows: An updraft region of tall convective clouds and intense rainfall with accompanying release of large amounts of latent heat (region III); a region of rapidly swirling winds corresponding to the large radial pressure gradient (region II); a boundary layer (region I) where the swirl winds interact frictionally with the sea surface, causing an inflow which supplies moist air to the updraft; and a warm, quiescent, relatively dry core, or eye, in which there is a very slow recirculation (region IV).

The swirling fluid of region II settles very slowly into the region below, supplying as it does so the fluid which moves radially inward in the boundary layer. There is almost no radial motion at all in II, and the flow therein is effectively frictionless.

Frictional effects are important in the boundary layer, region I, where the swirling flow loses some of its angular momentum to the sea surface. The radial component of the pressure gradient throughout the boundary layer is virtually the same as it is near the bottom of region II, but the frictionally depleted circumferential velocity in the boundary layer does not imply enough centripetal acceleration to balance that pressure gradient in I. Thus, the overall radial momentum balance is maintained in I only when the friction and momentum charges associated with a radial inflow are present.

The radial influx of fluid in I, whose source is the downdraft from II, moves into the annular region III where it flows upward and outward, conserving angular momentum. At any given radial position the updraft fluid has a deficit in *total* angular momentum, compared to the fluid in II at the same radius,

merely because of the frictional loss to the sea surface, which occurred in I. In the outer portions of the storm this deficit will appear as a negative circumferential velocity relative to the earth and, in fact, this high anti-cyclonic motion is always observed.

The fluid in the central core (IV) is relatively motionless. It is also very warm, so that at a given altitude the fluid is much less dense than the updraft fluid in III, which (for reasons explained below) is itself much less dense than nearby fluid in II. These differences in fluid densities in regions II, III, and IV imply that a column of air which is closer to the centre than a second column has less total weight than that more distant column; this is a necessary condition for the existence of the horizontal pressure gradient which balances the centripetal acceleration of the swirling flow in region II.

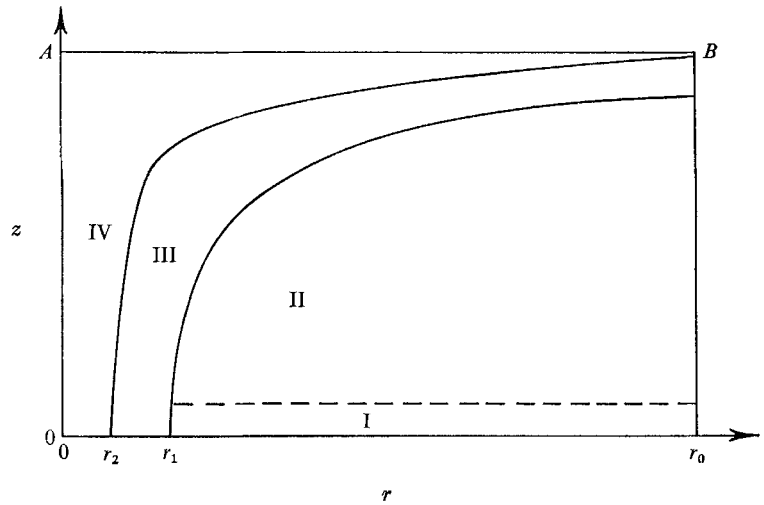

FIGURE 1. Schematic view of the hurricane.

The thermodynamic situation is depicted in figure 2. Curve 1 displays a typical pressure–temperature relation (from empirical observation) for a column of ambient, late summer tropical air (that along r_0–B in figure 1); this air is very moist at the lower altitudes due to high evaporation rates from the warm ocean surface. When air from the bottom of this column moves inward in the boundary layer and then upward in the updraft region, its moisture condenses (and falls out as rain) and the released heat of vaporization is retained by the rising air. The moisture in this air reaches saturation early on this journey, since the pressure and temperature drop almost adiabatically. The thermodynamic path for this process is given in figure 2 by curve 2, which displays the pressure–temperature relation for moist adiabatic expansion from ground level ambient conditions to some altitude B, which is chosen here as the 130 mb level. It seems completely logical to place the top of the container at that altitude above which the rising moist adiabat air would be denser than ambient air and below which the rising air would be less dense than ambient air. One sees that at a given altitude, the density must be smaller in region III than in region II.

The rising air in the updraft also entrains (frictionally) small amounts of air from the core and induces a slow recirculation in that core, with rising motion near the perimeter and settling in the centre. Probably, in fact, it is this recirculation that maintains the state of the gas in the core. The downward moving air would compress adiabatically (without re-evaporating any moisture) if there were no thermal exchange with the environment and, in the absence of such exchange, would consist largely of air compressed dry adiabatically from the state B of figure 2. Since there is some exchange with the adjacent air and water,

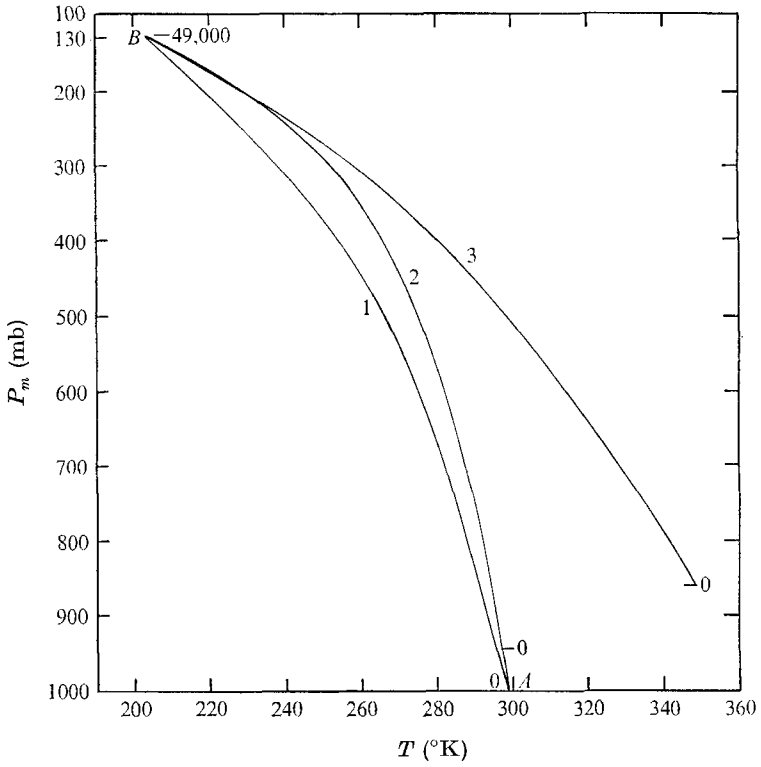

FIGURE 2. Thermodynamic loci. Curve 1 denotes the ambient p–T relation which was provided by Jordan (1957). The corresponding altitudes and densities are inferred using hydrostatics and the equation of state. Curve 2 denotes the p–T relation which obtains when gas in the state A is expanded *moist* adiabatically to lower pressures. Curve 3 denotes the p–T relation for air which is compressed *dry* adiabatically from state B of curve 2 to higher pressures.

the actual density in the core has a distribution which is intermediate between that of the dry adiabat and that of the moist adiabat. Using this hypothesis, curve 3 in figure 2 represents the pressure–temperature relation obtained by dry adiabatic recompression of gas from altitude B which has previously ascended along curve 2; the density of the gas in these states, having 'gone up' curve 2 to B and then down curve 3 is a lower bound on the locus of actual densities in the eye. This locus of thermodynamic states (curve 3 in figure 2) is easily obtained by invoking the equation of state, the requirements of

hydrostatic equilibrium, and a statement describing the temperature dependence of the saturation partial pressure for water vapour. In particular, one can calculate readily by these means the largest pressure discrepancy at ground level which is available to balance the centripetal acceleration of the swirl flow.

Given the dynamically consistent, self-sustaining model configuration described above, we must now ascertain whether quantitatively realistic flows occur. We restrict our attention to fluid motion in a uniformly rotating container of finite diameter and height. The container is chosen sufficiently large to enclose all phenomena associated with the storm. The motion is assumed axisymmetric throughout.† In the swirl region (II) the radial distribution of the circumferential velocity (or rather a family of such distributions) is assumed given with the requirement that the velocity must vanish at the outer edge of the container. The dynamics of the boundary layer determined by this external flow are governed by the full non-linear equations to which we return in a moment; in particular, this boundary-layer problem will determine the vertical velocity at the top of the boundary layer, which we expect to be negative, but small, over the outer section of the storm. Since there can be no radial inflow through the outer walls of the container, the boundary-layer inflow must originate entirely from the downdraft.

We do not treat the corner region (the boundary layer under the updraft region) where separation occurs and where the boundary-layer assumptions may break down, but insist that mass and angular momentum be conserved between the end of the boundary-layer region and the updraft region. In the updraft, non-viscous dynamics are taken as an adequate representation, with an imposed circumferential velocity distribution which goes smoothly from the maximum velocities (near $r = r_1$ in figure 1) to zero at the edge of the core. The fact that the fluids in the adjacent regions II and III have different angular momenta implies that the frictional coupling of the updraft flow to the main swirl flow is very weak and that very little diffusion of angular momentum occurs across the II–III interface. The very large horizontal scale associated with the overall flow (i.e the very small radial gradient of circumferential velocity) and the density discrepancies between the gas in II and the gas in III are consistent with such a loose coupling. Furthermore, any degradation of angular momentum in II by diffusion to III should readily be negated by an otherwise negligibly small radial inflow in II. If the weak coupling postulated here did not exist, it would be impossible to maintain swirl distributions of the sort described, and the flow would be restricted to a local recirculation in the neighbourhood of the updraft region rather than hurricane scale flows.

The model is assumed to be a quasi-steady model, in the sense that the boundaries of the regions change slowly with time as moist, rapidly circulating air from II is used up and III widens and settles; the storm feeds on its slowly diminishing initial store of angular momentum. The pressure is assumed to be constant radially across the top of the container (along AB in figure 1). The

† There are sizeable deviations from symmetry in real storms but it seems most unlikely that the inferences we draw here could be significantly altered by the consequences of such asymmetries.

locations of the boundaries between adjacent regions are determined by requiring continuity of pressure across them.

3. The boundary layer

The maximum velocities achieved either in or near the boundary layer are such that density changes within the boundary layer have negligible effect on the dynamics. (In no real storm will the Mach number exceed $\frac{1}{3}$.) The same statement does not hold for the thermodynamics, for which a fully compressible treatment must be used. Accordingly, the dynamics of the boundary layer (but not its thermodynamics) will be treated as though the fluid were incompressible (zero Mach number) with constant properties. Similarly, gravity plays a negligible role in determining the boundary-layer dynamics, due to the thinness of the fluid layer, so that while the ambient stratification must be included in estimates of the boundary-layer heat and moisture transport, the dynamic calculations will be carried out for an unstratified fluid.

The gradual changes which occur in the velocities and the geometry of the mature hurricane occur on a time scale much longer than one day. However, the thickest part of the boundary layer is in a region where the fluid motion relative to the earth is so slow that $h \simeq (\nu\Omega)^{\frac{1}{2}}$ and $t_0 \simeq h^2/\nu \simeq \Omega$, where Ω is the local normal component of the earth's rotational velocity (h is boundary-layer thickness, ν is the eddy diffusivity and t_0 is boundary-layer formation time). Thus, modifications of the boundary-layer structure which occur with a time scale of one day or longer are quasi-steady in character. Accordingly, we can conclude that boundary-layer formation or adjustment is not the rate controlling process in the continuing evolution of the mature storm, and we can use with confidence steady theory for the boundary layer itself.

Using a constant eddy viscosity, and a constant density, ρ, we write the steady-state conservation equations in a co-ordinate system which rotates with the container; i.e. the angular velocity of the co-ordinate system is the vertical component of the earth's angular velocity which, at 15° latitude, is given by $\Omega \simeq 1{\cdot}5$ rad/day. Since the ratio of the vertical scale to the horizontal scale is of order 10^{-3} we ignore horizontal diffusion compared to vertical diffusion and the conservation equations take the form

$$(ru)_r + (rw)_z = 0, \tag{3.1}$$

$$uu_r + wu_z - 2\Omega v - (v^2/r) + p_r = \nu u_{zz}, \tag{3.2}$$

$$u(rv)_r + w(rv)_z + 2\Omega ru = \nu(rv)_{zz}, \tag{3.3}$$

$$p_z + g = 0, \tag{3.4}$$

where u, v, w are radial, circumferential and vertical components of velocity, and p is the pressure divided by ρ. Equation (3.4) gives an incorrect view of the hydrostatic contribution to the pressure field but this plays no significant role in the boundary-layer dynamics.

We denote the circumferential velocity in region II by $V(r)$ and we note that

$$v(r, \infty) = V(r)$$

and, when (3.2) is applied to region II

$$p_r(r,\infty) = V^2/r + 2\Omega V. \tag{3.5}$$

Since p changes with z only by virtue of the hydrostatic effects implied by (3.4), we see that, in (3.2), p_r can be replaced by (3.5) and (3.2) becomes

$$uu_r + wu_z + 2\Omega(V-v) + (V^2-v^2)/r = \nu u_{zz}. \tag{3.6}$$

The following non-dimensional variables are convenient choices for the manipulation to follow:

$$\Psi = rV/\Psi_0, \quad \psi = rv/\Psi_0, \quad \phi = ru/\Psi_0,$$
$$z' = z/(\nu/2\Omega)^{\frac{1}{2}}, \quad w' = w/(2\nu\Omega)^{\frac{1}{2}}, \quad x = r^2\Omega/\Psi_0.$$

Ψ_0 is a dimensional quantity which characterizes the strength of the storm; it can be taken conveniently as $r_1 V(r_1)$ where r_1 is the value of r at or slightly outside of the radius of maximum velocity.

In terms of these variables (dropping primes immediately), (3.6), (3.3) and (3.1) become

$$\phi\phi_x + w\phi_z + (\Psi^2 - \psi^2 - \phi^2)/2x + (\Psi - \psi) = \phi_{zz}, \tag{3.7}$$

$$\phi\psi_x + w\psi_z + \phi = \psi_{zz}, \tag{3.8}$$

$$\phi_x + w_z = 0. \tag{3.9}$$

The boundary at $z = 0$ is relatively motionless and we will adopt the boundary condition which requires that ϕ, ψ and w must each vanish at $z = 0$. For a prescribed swirl flow $V = V(r)$ in the (inviscid) exterior region, the tangential momentum equation becomes

$$U[(rV)_r + 2\Omega r] \equiv 0.$$

Since the swirl distribution reported from observation and various laboratory experiments suggest that in the cases of interest here $V(r) \simeq r^{-n}$, where $n \simeq 1$, the appropriate accurate approximate boundary condition requires that $U = 0$. Hence for a given swirl distribution we have $\phi(x,\infty) = 0$, $\psi(x,\infty) - \Psi(x) = 0$.

All velocities decrease in magnitude as $x \to \infty$, so that for $x \gg 1$ we have $\Omega r \gg V$, and (3.7)–(3.9) become

$$\phi_{zz} = (\Psi - \psi),$$
$$(\Psi - \psi)_{zz} = -\phi,$$
$$w_z = -\phi_x.$$

Subject to the boundary conditions above, the solutions (which are the well-known Ekman profiles) are

$$(\Psi - \psi) + i\phi = \Psi(x)\, e^{-i^{\frac{1}{2}}z}, \tag{3.10}$$

$$w = \Psi_x(x) \int_0^z \sin(z/2^{\frac{1}{2}})\, e^{-z/2^{\frac{1}{2}}}\, dz. \tag{3.11}$$

Hence for the (3.7)–(3.9) we complete the boundary conditions by requiring that

$$\Psi - \psi + i\phi = \Psi\, e^{-i^{\frac{1}{2}}z} \tag{3.12}$$

when x is near the outer boundary of the container.

We can also carry out the asymptotic analysis for large z which we record here since it will be useful in obtaining the numerical solutions to the complete equations. If, as $z \to \infty$, $\phi \to \hat{\phi}$, $\Psi - \psi \to \hat{\psi}$ and $w \to W(x) + \hat{w}$, where $W(x) = w(x, \infty)$ and all quantities characterized by a $\wedge$ are small compared to unity, then the following linearization of (3.7) and (3.9) holds:

$$\hat{\phi}_{zz} = W\hat{\phi}_z + (1 + \Psi/x)\,\hat{\psi},$$
$$\hat{\psi}_{zz} = W\hat{\psi}_z - (1 + \Psi_x)\,\hat{\phi},$$
$$\hat{\phi}_x + \hat{w}_z = 0.$$

These have solutions:

$$\hat{\phi} = A_1(x)\, e^{-\lambda_1(x) z} \sin(\lambda_2(x)\, z) + A_2(x)\, e^{-\lambda_1(x) z} \cos(\lambda_2(x)\, z), \tag{3.13}$$

$$\hat{\psi} = B_1(x)\, e^{-\lambda_1(x) z} \cos(\lambda_2(x)\, z) + B_2(x)\, e^{-\lambda_1(x) z} \sin(\lambda_2(x)\, z). \tag{3.14}$$

Here A_1, A_2, B_1 and B_2 are arbitrary functions except that they must match to the large x solutions; that is

$$A_2(\infty) = B_2(\infty) = 0, \quad A_1(x \to \infty) = -B_1(x \to \infty) = -\Psi.$$

The functions λ_1 and λ_2 are given by

$$2\lambda_1 = (W^4 + 16\mu)^{\frac{1}{4}} \cos[\tfrac{1}{2} \tan^{-1}(4\mu^{\frac{1}{2}}/W^2)] - W, \tag{3.15}$$

$$2\lambda_2 = (W^4 + 16\mu)^{\frac{1}{4}} \sin[\tfrac{1}{2} \tan^{-1}(4\mu^{\frac{1}{2}}/W^2)], \tag{3.16}$$

where $\mu = (1 + \Psi/x)(1 + \Psi_x)$. When $|W| \ll 2\mu = O(1)$, as it is for the swirl flows of interest, then these solutions simplify with $\lambda_1 = \lambda_2 = \lambda = \mu^{\frac{1}{4}}/2^{\frac{1}{2}}$.

4. Maximum velocity estimates

The maximum velocities which can be obtained from the model configuration of figure 1 and the thermodynamic information of figure 2 can be estimated as follows. It is evident observationally that circumferential velocity distributions achieved in the swirl region approximately resemble $V = cr^{-n}$. The radial momentum equation just above the boundary layer (3.5) becomes

$$p_r \cong \rho c^2 / r^{2n+1}.$$

The density varies so little with radial position that (again) it may be taken to be a constant. Integrating from the edge of the container, $r = r_0$ (in figure 1) to the region of maximum winds, $r = r_1$,

$$p(r_0) - p(r_1) \cong \frac{\rho_0}{2n} \left(\frac{c}{r^n}\right)^2 = \frac{\rho_0}{2n} V^2.$$

Since the width of the updraft region is small compared to $r_0 - r_1$ and since $V(r)$ decreases rapidly with decreasing r in this region,

$$\frac{p(r_1) - p(r_2)}{p(r_0) - p(r_1)} \ll 1,$$

so that the maximum velocity achievable can be estimated as

$$V_{\max} = |(2n/\rho_0)\,(p(r_0) - p(r_2))|^{\frac{1}{2}}. \tag{4.1}$$

Estimates will be made for the extremes $n = \frac{1}{2}$ and $n = 1$. One observes that for a given pressure drop, the more rapidly decaying profile corresponds to larger

peak velocities, in good agreement with the observation that small storms (in the sense of the radial extent of the region of high winds) are often the most intense.

The pressure drop determined from curves 1 and 3 in figure 2 at $z = 0$ is $\Delta p \cong 140\,\text{mb}$, which corresponds to maximum velocities (using (4.1) of

$$V_{\max} = 100\,\text{metres/sec} \quad \text{for} \quad n = \tfrac{1}{2} \quad \text{and} \quad V_{\max} = 155\,\text{metres/sec} \quad \text{for} \quad n = 1.$$

Clearly the model configuration can support velocities which are considerably larger than those of real storms based solely on the thermodynamic properties of ambient tropical air. If the heat and moisture content of boundary-layer air entering the updraft region were substantially different from ambient conditions, as a result, for example, of heat and moisture gained from the sea surface while passing through the boundary layer, then these estimates will need to be modified (in the direction of higher velocities). We return to this point after the considerations of § 6.

The calculations above may be repeated for an alternative model in which there is no eye and the updraft extends clear to the origin; in this case the vertical pressure distribution at the centre is that corresponding to the moist updraft air, curve 2 of figure 2, and one obtains $\Delta p \cong 50\,\text{mb}$. However, if the updraft extends into the axis of symmetry the velocity distribution (very roughly) will be linear in r out to the point of maximum velocity and the pressure drop between r_0 and that point of maximum speed would be 25 mb. Thus, with $n = 1$, the maximum speed would be $V_{\max} = 62$ metres/sec. These results, when compared to those above, strongly suggest that a tropical storm can achieve hurricane proportions only if an eye is present in which some updraft air returns dry adiabatically down the central region so that re-compression results and the dynamic balance is maintained.

The above estimates do not depend on the radial extent of the storm nor are they very sensitive to the level chosen for the top of the storm. We emphasize that very large pressure differences can be supported when ambient tropical air is expanded moist adiabatically to some level associated with the top of the storm, and then recompressed adiabatically without moisture addition in part of the central column. *This latter step is crucial if very high velocities are to be achieved.* The fact that hurricanes do not achieve the enormous velocities calculated above is associated with the incomplete filling of the eye with dry adiabat air and with the fact that some heat is exchanged between air in the eye and its environment.

5. Numerical solution of the boundary-layer equations†

Attempts have been made by previous investigators to solve (3.7) and (3.9) for certain special cases. When the prescribed exterior swirl flow, $\Psi(x)$, is that of rigid body rotation, $\Psi = cx$ with constant c, (3.7)–(3.9) admit of separable solution of the form

$$\phi = xf(z), \quad \psi = xg(z), \quad w = -\int_0^z f(g)\,dg.$$

† The results presented in this section are derived and discussed in more detail in George (1970).

The ordinary differential equations governing f and g can then be integrated numerically (Lance & Rogers 1960); however, rigid body rotation is not a realistic model for hurricane swirls.

The flow under a realistic swirl has been treated approximately by use of the momentum integral method (Smith 1968). However, numerical studies of the boundary-layer equations in an *inertial* frame of reference (Anderson 1966) indicate that the momentum integral technique is not sufficiently accurate to predict reliably the vertical velocity at the top of the boundary layer, an extremely small but physically very significant quantity.

The boundary-layer equations in the rotating system do not yield to straightforward finite difference methods due to instabilities caused by the change of sign of the radial flux ϕ in some regions of the flow; in these regions (where $\phi > 0$), (3.7) and (3.8) assume the form of the heat equation with negative time-like co-ordinate, so that forward steps are no longer possible. It is, therefore, necessary to look for other more suitable numerical methods; in particular, we desire that our solution method be applicable for a wide variety of exterior swirls. A series expansion method in combination with the Galerkin technique is found to satisfy this requirement.

5.1. *The solution method*

Using the asymptotic solutions (equations (3.13)–(3.14)) as a guide, we adopt a set of suitable base functions $\{\omega_n(x, z)\}$, $n = 1, 2, \ldots$, with $\omega_n(x, 0) = \omega_n(x, \infty) = 0$. We assume that the solutions of (3.7)–(3.9) can be represented in D: $0 < x < \infty$, $0 \leqslant z < \infty$ in terms of these base functions by the series expansions

$$\phi = \sum_{n=1}^{\infty} a_n(x)\,\omega_n(x, z), \tag{5.1}$$

$$\psi = \Psi(1 - e^{-\lambda(x)z}\cos\lambda(x)\,z) + \psi', \tag{5.2}$$

$$w = -\frac{\partial}{\partial x}\int_0^z \sum_{n=1}^{\infty} a_n(x)\,\omega_n(x, \zeta)\,d\zeta, \tag{5.3}$$

$$\psi' = \sum_{n=1}^{\infty} b_n(x)\,\omega_n(x, z). \tag{5.4}$$

The first term in the expression for ψ is introduced so that the functions† ϕ and ψ' represented by the series expansions satisfy homogeneous boundary conditions; ϕ and ψ' belong to the class s of continuously differentiable functions f defined in the interval $0 \leqslant \zeta < \infty$ and having the properties

$$\int_0^{\infty} f^2 d\zeta < \infty, \quad f(0) = 0, \quad f \sim e^{-\zeta}\sin\zeta \quad \text{as} \quad \zeta \to \infty.$$

A series of numerical experiments (George 1970) has shown that the base functions

$$\omega_n(\zeta) = \frac{1}{H_n^{\frac{1}{2}}} \sum_{k=1}^{n} g_{nk}\, e^{-k\zeta}\sin k\zeta,$$

† We note that when ϕ is known, w is determined from the integral (5.3) of the continuity equations.

can be used to approximate arbitrary functions in s; here g_{nk} and H_n are orthonormalizing coefficients for the set $\{e^{-k\zeta}\sin k\zeta\}_{k=1}^{\infty}$ such that

$$\int_0^\infty \omega_n \omega_m \delta\zeta = \delta_{nm},$$

the Kronecker delta. The approximations of trial functions were carried out in the least square sense, but the resulting pointwise errors were found small compared to the function values. Similarly the coefficients of the expansions in terms of $\omega_n(\zeta)$ converged rapidly as n increased.

The base functions for the expansions (5.1) and (5.4) are therefore chosen as

$$\omega_n(x,z) = \sum_{k=1}^{n} g_{nk}\, e^{-(k\lambda(x)z)} \sin(k\lambda(x)z) \quad (n = 1, 2, 3, \ldots) \tag{5.5}$$

with

$$\int_0^\infty \omega_n \omega_m dz = H_n \delta_{nm}/\lambda(x).$$

With this representation the series equations (5.1)–(5.3) are substituted into the boundary-layer equations (3.7)–(3.8). The Galerkin technique is used to make the residuals small compared to unity; thus

$$\left.\begin{aligned} \int_0^\infty \omega_n(x,z)\, \mathscr{L}_1(\phi,\psi,w) = 0 \\ \int_0^\infty \omega_n(x,z)\, \mathscr{L}_2(\phi,\psi,w) = 0 \end{aligned}\right\} \quad (n = 1, 2, 3, \ldots) \tag{5.6}$$

where $\mathscr{L}_1(\phi, \psi, w) = 0$ and $\mathscr{L}_2(\phi, \psi, w) = 0$ are the radial and peripheral momentum equations, (3.7) and (3.8). This yields a set of ordinary differential equations for the coefficients $a_n(x)$ and $b_n(x)$.

Starting from the Ekman-layer values for a given swirl at large x, the ordinary differential equations were integrated numerically towards the origin using a Haming predictor-corrector routine with Picard starting iteration. The following numerical experiments were done to ensure that the results obtained are correct:

(1) For a given swirl and a fixed number of terms, N, in the series approximation (usually $N = 1$ or 2), the equations were integrated inward in x starting from different points, x^∞, until the coefficients a_i, b_i became independent of the starting point to at least five decimal places. The least value of all the starting points used for which a_i and b_i did become independent of the starting point was regarded as the Ekman-layer edge or the initial point for the integration. In most cases this was found to be near $x = 5$.

(2) Experiment (1) was repeated for different step sizes, mostly within the range $O(10^{-3}) \leqslant L \leqslant O(10^{-2})$. It was found changes in the step size did not affect the results of experiment (1) up to five decimal places, for those step sizes for which the Picard starting iteration converged.

(3) Using the initial point and a suitable step size determined from the above experiments, the equations were integrated with higher values of N until the higher-order coefficients a_N, b_N became less than one percent of a_1 and until the downdraft at the top of the boundary layer ($w(x, \infty)$) became independent of N

up to three decimal places. In most cases this convergence was achieved with $N = 2$ or 3.

A final check was made by doing some cases of experiments (1) and (2) for $N = 3$; these were found to make little or no difference in the initial points established for $N = 1$. Experiments (1) and (2) were done extensively for the swirls $\Psi = x^{0.1}$ and $\Psi = 1$. For the other swirls treated, a few cases of experiments (1) and (2) were done. Experiment (3) was done for all swirls treated.

The residuals were computed and were found to be of $O(10^{-3})$ for z less than the e-folding thickness, $1/\lambda$, of the boundary layer and are therefore small compared to ϕ_{zz} which is of $O(1)$ in this region. Finally, since

$$\phi_{zz}(x, 0) = \Psi(1 + \Psi/x),$$

a known function, the error of this quantity due to the approximation process was computed and found to be one percent or less for the main boundary layer ($x <$ starting point but $x >$ the region of strong updrafts).

By virtue of all the foregoing checks – small residuals, converging coefficients and small errors in $\phi_{zz}(x, 0)$ – the results obtained are considered reasonably good approximations to the solutions of the boundary-layer equations. In particular, the calculation gives an excellent estimate of the total vertical flux of fluid into the boundary layer and this flux is the *only* quantitative result of the analysis which is needed in our calculation of the overall dynamic-thermodynamic balance.

5.2. *Discussion of numerical results*

The preceding solution method was applied to a variety of prescribed exterior swirl distributions and we present here the results of a few cases. As mentioned earlier, swirls observed in hurricanes seem to be of the form $v = cr^{-n}$ with $\frac{1}{2} \leqslant n \leqslant 1$; this law cannot hold as $r \to \infty$, since that would imply an infinite angular momentum (relative to the earth) associated with the storm. We avoid these difficulties if we require that the peripheral velocity vanish at a finite radius r_0. A simple case is that of linear decay beyond a given radius r':

$$\left.\begin{aligned} v &= c_1/r && (0 < r \leqslant r'), \\ v &= c_2(r_0 - r) && (r' \leqslant r < r_0). \end{aligned}\right\} \tag{5.7}$$

Imposing continuity of velocity and stress at $r = r'$, (5.7) becomes in non-dimensional form

$$\Psi = \begin{cases} 1 & \text{in} \quad 0 < x \leqslant \frac{1}{4}x_0 \\ 4((x/x_0)^{\frac{1}{2}} - x/x_0) & \text{in} \quad \frac{1}{4}x_0 \leqslant x \leqslant x_0. \end{cases}$$

Since this swirl vanishes at x_0, it introduces a singularity in the differential equations at that point. Using the first terms of the series expansions (5.1)–(5.4), we investigated the behaviour of the solutions near the singular point with the usual Taylor expansion method. In this region the solutions closely approximate the Ekman-layer solutions (3.10)–(3.12) so that the starting procedures used for the numerical integrations were exactly those described above.

In interpreting the (non-dimensional) results, we choose as typical values for the parameters: $\nu = 10^5\,\mathrm{cm}^2/\mathrm{sec}$; $V_{\max} = 150$ miles/hour at $r_1 = 20$ miles;

$\Psi_0 = r_1 V_{\max}$; effective angular velocity of the earth at 15° latitude $\Omega = \frac{3}{2}$ radians/day. For brevity, the vertical velocity at the top of the boundary layer, $w(x, \infty) = W$, will be referred to as the downdraft, when $W < 0$, and updraft, when $W > 0$.

The downdraft induced by the swirl (5.8) is displayed in figure 3. There is a large region of slowly-varying weak downdraft surrounding a small region of strong updraft near the centre. The downdraft extends from the edge of the storm ($r_0 \cong 1000$ miles) to about $r = 200$ miles where it becomes updraft;† until about $r = 100$ miles the updraft is very small, but inward of this position it increases very rapidly. The maximum downdraft is $-W = 0{\cdot}266$ cm/sec.

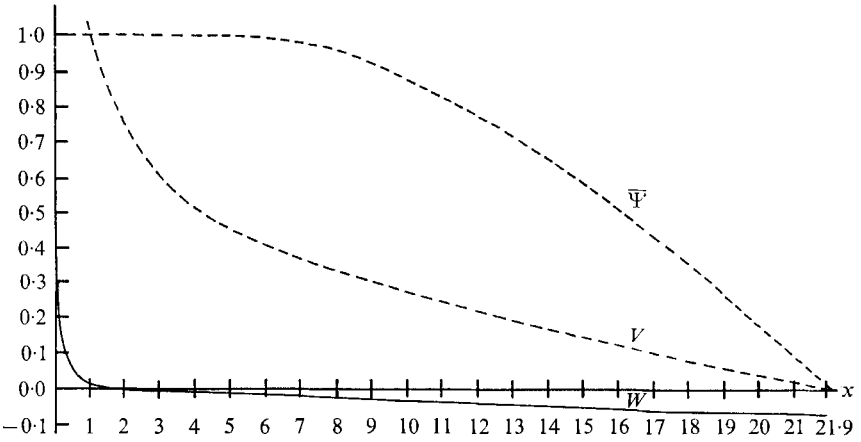

FIGURE 3. Ψ, V and W *vs.* x for the swirl pattern.

$$\Psi = \begin{cases} 1 & (0 < x < 5{\cdot}5). \\ 4\left(\left(\frac{x}{22}\right)^{\frac{1}{2}} - \frac{x}{22}\right) & \text{in} \quad (5{\cdot}5 < x < 22). \end{cases} \tag{5.8}$$

The radial, circumferential, and vertical velocity profiles induced by the swirl (5.8) are shown in figures 4, 5, and 6. The radial velocity field shows an inflow layer of the order of one mile in vertical extent (the e-folding thickness is closer to 1800 feet) with an outflow layer of very slow radial velocity above the inflow layer. At each radius the maximum radial velocity is about one-third the maximum peripheral velocity. These velocities increase with decreasing radius, slowly at first and then more rapidly as the centre is approached. We do not expect that these results are accurate in the region of strong updrafts, since the boundary-layer assumptions are no longer valid there.

The vertical velocity is everywhere downward in the downdraft region, with maximum velocity attained at the top of the boundary layer.

In a hurricane one does not know the exact swirl distribution, and it need not be the same for all huricanes, so it is necessary to demonstrate that the overall

† By the time this paper was in its final stages of preparation, further studies had revealed that this early updraft was an antifact of the methodology. However, the downdraft in $200 < r < 1000$ miles is sufficiently accurate that no revision is needed for the purposes of this paper.

characteristics of the flow pattern are insensitive to small variations in the prescribed swirl. We have tested the sensitivity of the downdraft to the details of $\Psi'(r)$ using several different $\Psi'(r)$. The details are given in George (1970). In brief, these studies confirm that the downdraft is *not* sensitive to those details.

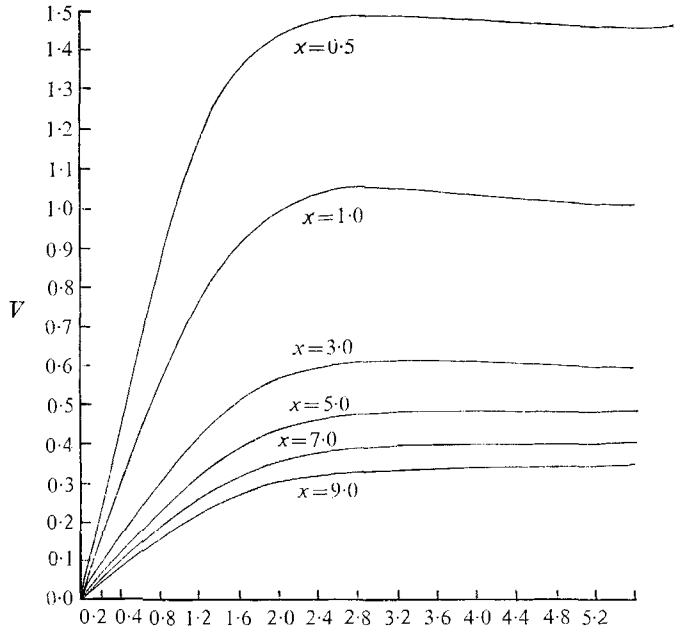

FIGURE 4. Circumferential velocity profile in the boundary layer for the Ψ' of figure 3.

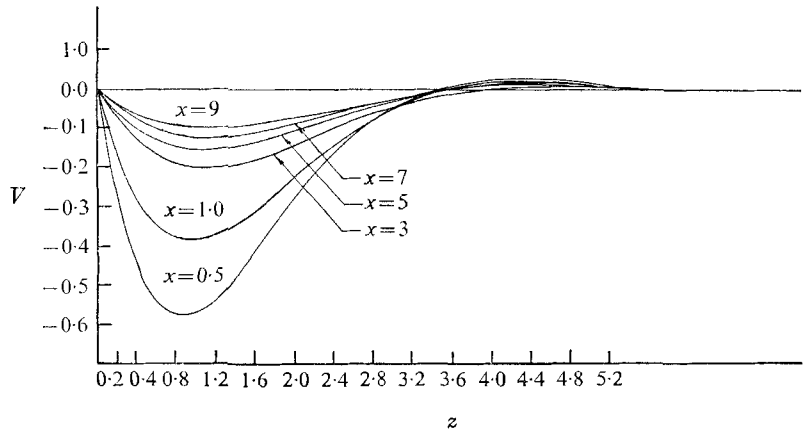

FIGURE 5. Radial velocity distribution in the boundary layer for the Ψ' of figure 3.

We conclude that there exists a family of physically reasonable swirls for which the radial inflow to the storm is produced in a large region of weak downdraft, inside of which there is a narrow region of strong updrafts. We have shown, furthermore, that this general picture is stable with respect to small changes in the swirl distributions, and we believe that any self-contained model of the storm must involve swirls qualitatively similar to that of (5.8), which decay in a finite radius.

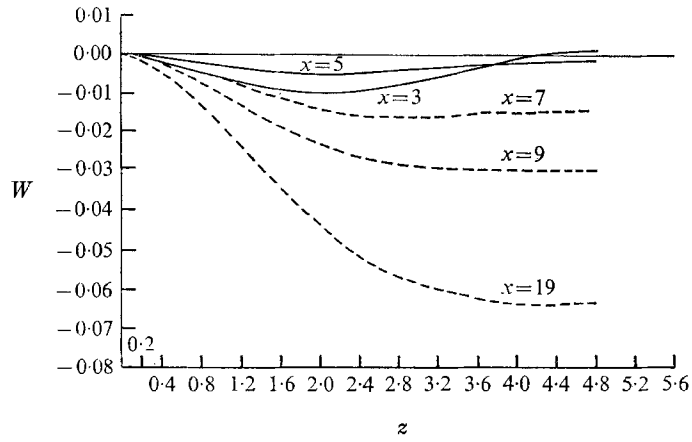

FIGURE 6. Vertical velocity distribution in the boundary layer for the Ψ of figure 3.

6. Estimates of boundary-layer heat and moisture transfer†

It is widely known that rotating fluids behave differently in many ways from non-rotating fluids, but it is less widely appreciated that heat and mass transfer due to forced convection may also be markedly different in rotating boundary layers from in non-rotating problems. This being the case, it is a doubtful practice at best to estimate such transfers in rotating systems by means of formulas based intuitively on the non-rotating flat-plate problem; instead it is desirable to arrive at estimates based on the governing equations, even if only approximate calculations can be done.

The present problem, i.e. the boundary-layer heat and moisture transfer from the warm sea surface in the mature hurricane, is an important instance of such rotating flows. There are in actuality two problems involved in sorting out the energetics of the storm. In the first place there is the ambient air–sea energy conversion cycle; radiative heating of the upper layers of the sea; consequent evaporation of water at the sea surface; upward transport of the water vapour by turbulent mixing or convective cumulus clouds; heating of the air by release of latent heat of condensation; and finally, radiative cooling of the atmosphere to space.

Secondly, there is the influence of the intense swirling flow associated with the storm and the resultant boundary-layer velocities on the air–sea energy transport processes. Although it is this latter problem of boundary-layer energy transfer under a swirling flow that is significant for the hurricane, it will be necessary to model the ambient air-sea interaction processes in order to adequately discuss hurricane energetics, since these ambient processes are in fact a dominant feature of the energy balance in the tropics.

The wind fields of the storm are determined by the cyclone scale thermodynamics (the radial pressure drop and the release of latent heat in the updraft),

† The results presented in this section are derived and discussed in more detail in Hammond (1970).

but these winds are locally independent of the energetics of the flow. This means that the velocity profiles in the boundary layer may be prescribed independently of the local heat and moisture transfer (forced convection), although the converse is not true. However, we do not expect that the heat and mass transfer will depend sensitively on the exact velocity profiles used, as long as they are qualitatively correct. We therefore adopt analytically convenient approximate profiles for the boundary layer which retain the main features of the solutions found in the previous section, choosing the radial velocity in the form

$$u = a \sin(\lambda z)\, e^{-\lambda z}$$

and w is determined from the continuity equation (3.1).

Here a and λ are functions of the radial co-ordinate; these functions are chosen so that the downdraft at the top of the boundary is uniformly distributed in r over the outer region of the storm and so that the maximum radial velocity is distributed in r like

$$|u_{\max}| = \tfrac{1}{3} V(r),$$

where V is the prescribed exterior swirl flow given by (5.8). These simplifications, qualitatively good approximations to the true situation, are accurate enough for the present investigation.

6.1. *The energy equation*

The condensation of even small amounts of water vapour releases large amounts of latent heat to the atmosphere, and this is in fact the main source of heat to the atmosphere. Even in saturated air, however, the concentration of water vapour is less than 2·5% by weight, and is usually much less for the temperatures prevailing in most of the atmosphere. Thus even though the heat capacity of water vapour is about twice that of air, the water vapour plays an important role in heat transfer *only* as a source of latent heat. We will make use of this fact by formulating an energy equation for dry air, idealized as a perfect gas, and by keeping track of the moisture content (through the equations of mass conservation) as a potential heating source.

Radiation is also an important energy transfer mechanism in the atmosphere, but no explicit radiative calculations will be done here. However, the net radiative transfer to the atmosphere is usually negative, so that net radiative effects may be modelled by including an energy sink in the energy equation.

With the assumption of local thermodynamic equilibrium, so that the thermodynamic functions and their relations for a closed system may be introduced, the energy equation for a fluid may be written (Goldstein 1960, p. 42):

$$T\frac{dS}{dt} = \frac{Dh}{Dt} - \frac{1}{\rho}\frac{Dp}{Dt} = \frac{1}{\rho}\Phi + \frac{1}{\rho}\nabla.\mathbf{q} + Q + R. \tag{6.1}$$

This equation states that the change in entropy (S) equals the viscous dissipation (Φ), the divergence of the conductive heat flux (q), and the rate of heat addition per unit mass due to chemical reaction (Q) and radiation (R). For forced convection, it is usually convenient to choose the enthalpy (h) as one of the thermodynamic variables, and we will do so here. We specialize to the case of a

perfect gas, for which $dh = c_p dT$, and introduce the Prandtl number, $P_r = \mu c_p/k$, and the Schmidt number, $S_c = \mu/\rho D$. We also assume quasi-steady processes, such that $D/Dt = u\,\partial/\partial r + w\,\partial/\partial z$, and neglect lateral diffusion compared to vertical diffusion, exactly as in the previous sections.

With these simplifications we may write the following expressions for the terms on the right-hand side of (6.1) (neglecting R for now)

$$\frac{1}{\rho}\nabla.q = \frac{1}{\rho}\frac{\partial}{\partial z}\left(\frac{\mu}{P_r}\frac{\partial h}{\partial z}\right), \tag{6.2}$$

$$\frac{1}{\rho}\Phi = \frac{\mu}{\rho}\left[\left(\frac{\partial u}{\partial z}\right)^2 + \left(\frac{\partial v}{\partial z}\right)^2\right], \tag{6.3}$$

$$Q = \frac{L.r_A}{\rho} = L.\left[-\frac{Dy}{Dt} + \frac{1}{\rho}\frac{\partial}{\partial z}\left(\frac{\mu}{S_c}\frac{\partial y}{\partial z}\right)\right]. \tag{6.4}$$

Here, L is the heat of vapourization for water, $-r_A$ is the rate of loss of water vapour in the fluid due to chemical reaction, y is the mass fraction concentration of water vapour ρ_A/ρ, and we have used the equation of conservation of water vapour (with y neglected compared to unity) to express the rate of heat addition due to condensation.

If we combine the energy equation with the equations of motion, (3.1)–(3.3), we obtain

$$\frac{D}{Dt}(h + Ly + \tfrac{1}{2}(u^2+v^2) + gz) = \frac{1}{\rho}\frac{\partial}{\partial z}\left[\frac{\mu}{P_r}\frac{\partial h}{\partial z} + \frac{\mu}{S_c}\frac{\partial y}{\partial z} + \frac{\mu\,\partial(\tfrac{1}{2}(u^2+v^2))}{\partial z}\right] + R. \tag{6.5}$$

We note the *exact* cancellation of the frictional dissipation and pressure terms in (6.5). With the further assumptions that $P_r = S_c = 1$ (constants) and that μ is independent of z, we can define a new energy function involving the stagnation enthalpy ($h_0 = h + \frac{1}{2}(v^2+u^2)$), the latent heat energy Ly, and the potential energy gz,

$$H = h_0 + Ly + gz \tag{6.6}$$

for which the energy equation becomes

$$u\frac{\partial H}{\partial r} + w\frac{\partial H}{\partial z} = \nu\frac{\partial^2 H}{\partial z^2} + R. \tag{6.7}$$

It is this equation, derived for a real fluid, that is taken to model the energetics of the turbulent, geophysical fluid. The assumptions $P_r = S_c = 1$ and $\mu \neq$ const imply a similarity in the turbulent transport processes for mass, momentum and heat and imply not only that the respective eddy coefficients are equal to each other, but that they can be taken as constant with height over the dynamic boundary layer. While very little can be stated with certainty, there is some evidence (Priestley 1959) that these assumptions are reasonably good for forced convection estimates over water in which the scale of the investigation is large compared to individual events (such as cumulus clouds) and in which the interest is on the magnitude of the heat flux penetrating to various levels. In any case these assumptions are qualitatively correct and will be accurate enough for present purposes.

The release of latent heat in the atmosphere occurs largely in individual cumulus clouds. On the scale of the hurricane, however, such discrete events are too small to be included. Instead, use is made of the fact that the strong turbulent mixing results, on the average, in smooth lateral profiles of temperature and moisture (such smooth profiles are reported observationally in the swirl regions of hurricanes). It is therefore adequate to represent the moisture transport, and hence the transport and release of latent heat, as a turbulent diffusive process in the vertical direction. The local lateral mixing assumed here does not contradict the neglect of lateral diffusive terms in the equations; on the cyclone scale, lateral diffusion plays no significant role in the energetics of the storm.

The energy function H introduced here (equation (6.6)) can be interpreted as the sum of the geopotential energy and a 'moist' stagnation enthalpy. By its derivation, it is that function which is constant during changes of state (of a unit mass of moist air) for which the only entropy change is that due to release of latent heat (moist adiabatic processes). With the non-dimensionalization of § 3, (6.7) becomes

$$\phi H'_x + w' H'_{z'} = H'_{z'z'} + R', \tag{6.8}$$

where $H' = H/H^*$, $R' = R/(2\Omega H^*)$, with H^* to be chosen later.

Since the conductive capacity of the ocean is effectively infinite compared to that of the air, the sea surface is isothermal ($T(0, x) = T_s$) and the water vapour concentration at the surface is saturated at that temperature ($y(0, x) = y_s^*(T_s)$); the boundary condition at $z = 0$ states that $H(0, x) = H_s$, a constant, except in the innermost regions of the storm where the variation of y^* with pressure should be included. The boundary condition at the top of boundary layer ($z \to \infty$) states that $H \to H_a(z)$, the ambient energy profile for the tropical atmosphere; we can best make this requirement more explicit after discussing the ambient situation.

6.2. *The ambient atmosphere*

In the absence of a storm, or at the edges of a storm, we expect the ambient energy profile in the vertical to be that of the late summer tropical troposphere, for which the energy profile has on the average the characteristic shape given in figure 7. This profile is not a static distribution but is actively maintained by a continuing supply of sensible and latent heat from the warm sea surface, by vertical diffusion (in which we include cumulus convection), and by radiative loss to space. It is therefore important to include these ambient processes explicitly in a model of the energetics of a storm.

In the ambient profile (figure 7), the region above the elbow can have little influence on processes in the boundary layer, since there can be no net diffusive transport of energy across the elbow. We therefore adopt an idealized form of the ambient profile (figure 8) which is asymptotic to a constant (H_∞), as $z \to \infty$. Since the upper air is assumed to be colder in this approximation than it actually is, this idealized profile provides a lower bound on the energy available in such an atmosphere. It is convenient to use these empirically based profiles and an observational value (Malkus 1962, p. 112) for the ambient energy flux at the sea surface ($F_s = -\rho\nu(dH/dz)|_{z=0}$), typically $1{\cdot}8 \times 10^5$ ergs/cm^{2}sec, to fit a value of the eddy coefficient, ν; we find $\nu = 2{\cdot}7 \times 10^5$ cm^2/sec, in good agreement

with estimates of bulk eddy coefficients by other authors for corresponding conditions (Priestley 1959, p. 100).

In the absence of a storm the ambient profile modelled by figure 8 arises as a

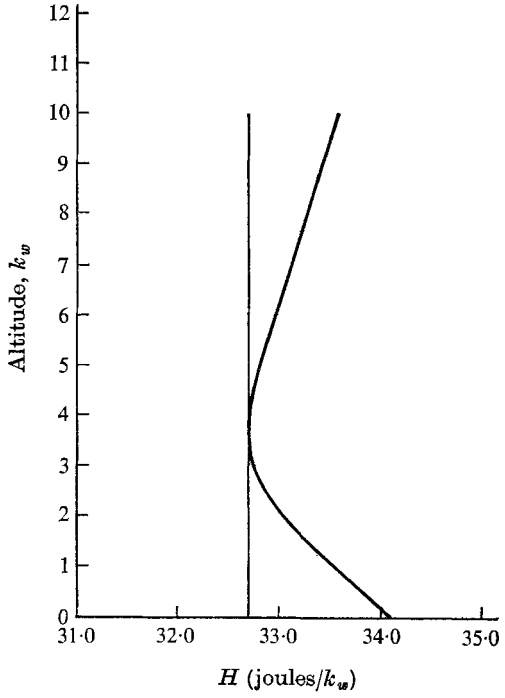

FIGURE 7. A typical ambient total enthalpy profile for the real atmosphere.

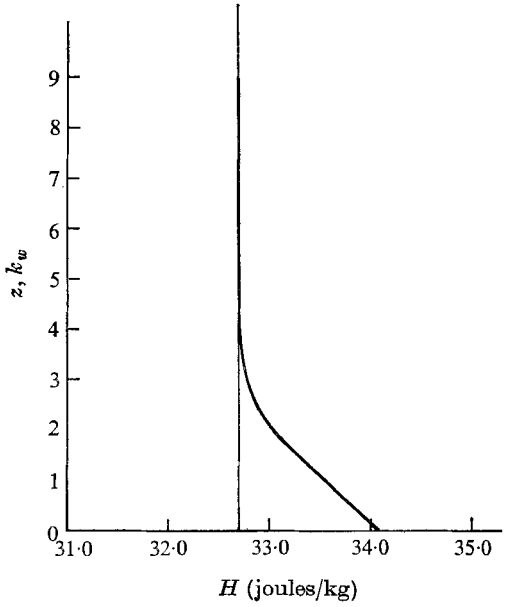

FIGURE 8. The enthalpy profile adopted for the enthalpy transport analysis of this paper.

result of a balance between the terms on the right-hand side of (6.8). Using the subscript a to refer to this ambient condition, we have

$$\eta_{az'z'} + R'' = 0, \tag{6.9}$$

where $\eta = (H - H_\infty)/(H_s - H_\infty)$ and $R'' = R'/(H_s - H_\infty)$. According to (6.9), we may estimate the net radiative heat loss from the fluid by the vertical divergence of the energy flux associated with a given ambient profile. For the profile of figure 7, the radiative cooling is maximum near the elbow (mid-troposphere) and small in the boundary layer and upper troposphere.

In the presence of a storm or other non-ambient situation, we expect that R will depend in part on the existing profile (η rather than η_a); that is, we expect that R will change as the profile changes. We therefore adopt the following somewhat arbitrary but simple model for R,

$$R'' = -f(z).\eta(z), \tag{6.10}$$

where $f(z)$ is determined by (6.9). Thus,

$$f(z) = \eta_{az'z'}/\eta_a \tag{6.11}$$

for a particular ambient profile. We might equally well choose a different functional dependence on η (e.g. R'' might be proportional to η^2) in (6.10). We do not, however, expect the final results to depend heavily on the particular form chosen; this expectation is verified later in numerical calculations.

With the inclusion of the above model for the radiative energy sink, the energy equation (6.8) becomes (dropping primes)

$$\phi\eta_x + w\eta_z - \eta_{zz} + f(z)\,\eta = 0, \tag{6.12}$$

with boundary conditions

$$\left.\begin{aligned} \eta(x, 0) &= 1, \\ \eta(x_0, z) &= \eta_a(z), \\ \eta \to 0 \quad &\text{as} \quad z \to \infty. \end{aligned}\right\} \tag{6.13}$$

This equation has been solved approximately for a number of choices of ambient profile, $\eta_a(z)$; here we present the results for the three cases (displayed along with the empirically based profile in figure 9):

(1) $\eta_a = 0.$

(2) $\eta_a = e^{-z/h}.$

(3) $\eta_a = \operatorname{erfc}(z/h).$

The first case is that of zero ambient profile ($R = 0$). For consistency the parameter h in cases (2) and (3) was chosen as 2·8 and 3·16 respectively (non-dimensional units) so that the ambient flux at the sea surface agrees with the observational value given earlier (this is simply a means of specifying a particular profile or a particular ambient situation; the results do not depend significantly on the particular value of the flux which is used).

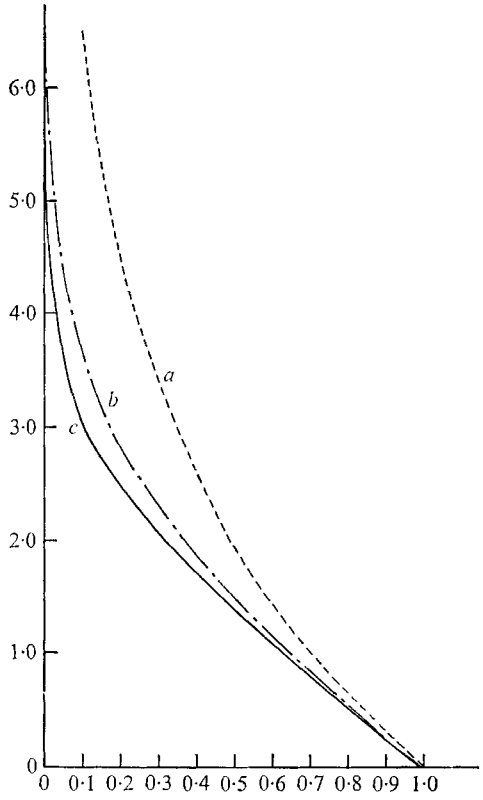

FIGURE 9. Total enthalpy profiles: (*a*) η_a for case (2), (*b*) η_a for case (3), (*c*) η_a from figure 8.

6.3. *Solution method and results*

We obtain approximate solutions to (6.12) by means of a modified Oseen method. The method consists in replacing the convective terms $\phi\eta_x + w\eta_z$ by the single term $\overline{w}\eta_z$,† where $\overline{w}$ is some z-averaged value of the vertical velocity w. After the solution of the resulting approximate equation is obtained with $\overline{w}$ as a parameter, $\overline{w}$ is determined by a consistancy calculation which picks out the best $\overline{w}$ in an average sense

$$\int_0^\infty (\phi\eta_x + w\eta_z)\, dz = \int_0^\infty \overline{w}\eta_z dz. \tag{6.14}$$

Equation (6.12) becomes

$$\overline{w}\eta_z - \eta_{zz} + f(z)\,\eta = 0. \tag{6.15}$$

For case (1) above $f(z) \equiv 0$ and we have

$$\eta = e^{-|\overline{w}|z}. \tag{6.16}$$

† As will appear, it is $w\eta_z$ rather than $\phi\eta_x$ which is the dominant convective term, since although w is very small compared to ϕ, η_x compared to η_z is even smaller and the solution is only weakly dependent on x.

Estimating $\overline{w}$ from the consistency calculation, we find (figure 10) that $\overline{w}$ is a slowly-varying function of x whose magnitude is everywhere $< |W|$ (W is the downdraft at $z \to \infty$) and decreases as x decreases. In dimensional terms the exponent in (6.16) is $(\overline{w}/\nu)z$, where $\nu/\overline{w}$ is the height scale associated with changes in the ambient energy profile due to forced convection; for $\nu = O(10^5\,\mathrm{cm^2/sec})$ and $\overline{w} = O(W) \sim 0{\cdot}1\,\mathrm{cm/sec}$ (consistent with the results of § 5), this height is about ten kilometres. Hence the solution (6.16) is effectively constant through the boundary layer, implying that the convection changes the ambient energy profile very little at all in the region of interest (the lowest few kilometres).

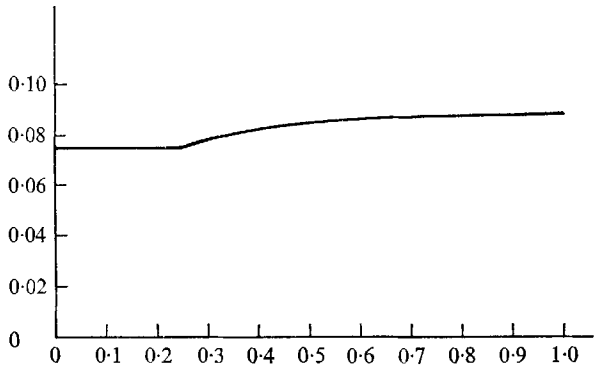

FIGURE 10. Oseen-averaged non-dimensional vertical velocity $\overline{w}$ *vs.* radial co-ordinate x/x_0.

The flux from the sea surface is given by

$$F_s = -\rho\nu \left.\frac{\partial H}{\partial z}\right|_{z=0} = \rho(\nu 2\Omega)^{\frac{1}{2}}(H_s - H_\infty)\,|\overline{w}| \tag{6.17}$$

and represents, for case (1), only the forced convection contribution, since in this case the ambient flux is zero. With $\Delta H = 1{\cdot}0 \times 10^8\,\mathrm{ergs/g}$ (corresponding to $\Delta T = 4\,^\circ\mathrm{C}$, $\Delta y = 0{\cdot}0025$), and $\nu = 10^5\,\mathrm{cm^2/sec}$, the flux is

$$F_s = 1{\cdot}94 \times 10^4\,\mathrm{ergs/cm^2\,sec};$$

this is an order of magnitude smaller than the ambient observational value reported earlier, implying that the contribution of the forced convection to the energy supply of the storm will be small compared to the contribution of the processes which maintain the ambient energy profile.

It may be argued, however, that the intensity of the turbulent mixing, hence the eddy coefficients, increase with increasing velocities, hence decreasing x, and that this would have the effect of increasing F_s with decreasing x. We can check this assertion, since the solution method used here can be applied for x-dependent diffusivities. We find that to a first approximation, the flux is unchanged from that given above; if ν varies by a factor of three between $x = x_0$ and $x = \frac{1}{4}x_0$ the increase in the flux is nowhere more than a few per cent.

Case (2) includes the ambient processes, although the model is not very realistic since the net radiative loss in this case is maximum at $z = 0$, rather than in

midtroposphere; however, its simplicity makes it a convenient example. The solution to (6.15) for this case is ($|w| \ll 1$)

$$\eta = \exp\{-z/h[\tfrac{1}{2}|\overline{w}|\,h + (1+\tfrac{1}{4}\overline{w}^2h^2)^{\frac{1}{2}}]\} \cong \eta_a(z)\exp(-\tfrac{1}{2}|\overline{w}|\,z). \tag{6.18}$$

Here $\overline{w}$ (again computed from (6.14)) is a slowly varying function of x as before with $|w| \leqslant |W|$, so that it will be sufficient to show results for this upper bound. The energy profile in the boundary layer is depressed slightly (figure 11) from its ambient values. The interpretation given previously of $1/\overline{w}$ ($\nu/\overline{w}$ dimensionally) as the appropriate scale height for changes of the profile from ambient is confirmed. The forced convection in the outer region† of the storm *lowers* the energy content

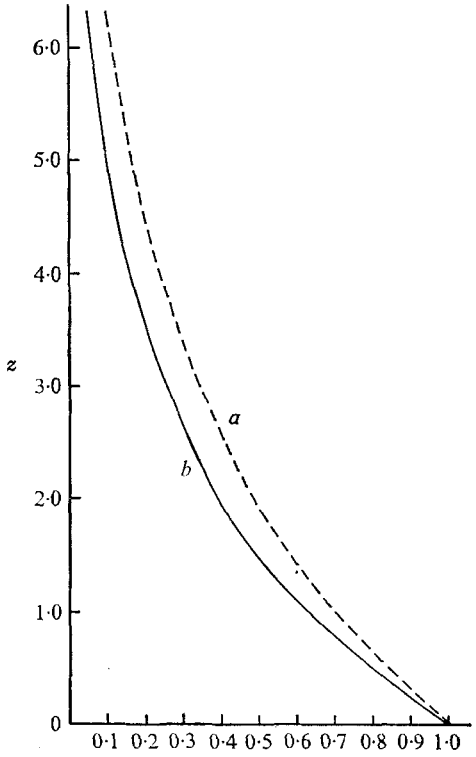

FIGURE 11. Enthalpy profile with downdraft: (*a*) ambient profile for case (2); (*b*) profile with $\overline{w} = -0{\cdot}1$.

of the boundary-layer air slightly and *increases* the flux at the sea surface by a small amount (approximately by the factor $(1+\frac{1}{2}W)$, or at most 5 % for $W = 0{\cdot}1$).

The results above are qualitatively duplicated when we proceed to case (3), which has a more realistic distribution of radiative cooling. For particular values of $\overline{w}$, (6.15) is conveniently solved numerically using a double-sweep method; standard centred-difference formulas are used for the derivatives in the finite-difference scheme. The semi-infinite domain was truncated at some large value

† These models do not apply near the updraft region, and do not strictly apply for x smaller than the crossing point where W changes sign; they can, however, be interpreted to apply for small positive $\overline{w}$ if the solution is rewritten as

$$\eta \cong \eta_a(z)\, e^{\frac{1}{2}\overline{w}z}.$$

of z, z^*, and the boundary condition at infinity applied there. For large enough z^*, the error introduced by this truncation is negligible, as was confirmed by using the method for the case $\overline{w} = 0$, for which the exact solutions are just the ambient profiles. The results obtained from this method are plotted in figure 12 for $\overline{w} = 0$ (the ambient profile) and $\overline{w} = 0{\cdot}1$. The profile depression is even less for this more realistic model than that depicted in figure 10. Only for extremely large downdrafts, an order of magnitude larger than those considered here, will the convection substantially depress the ambient profile.

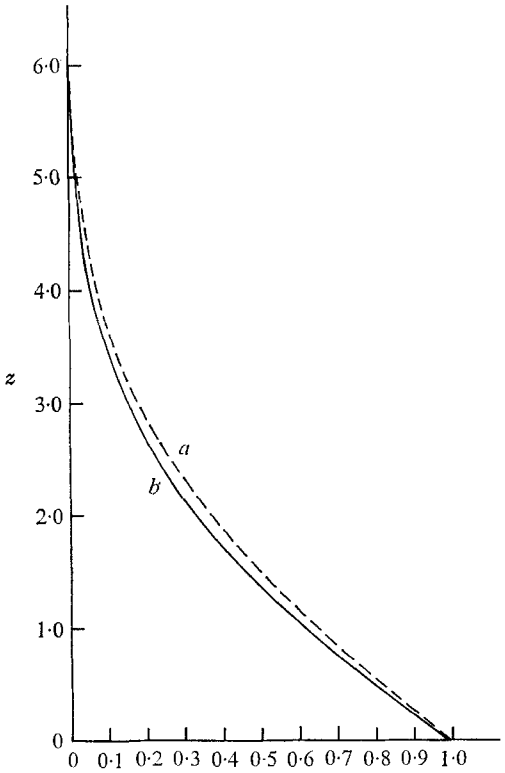

FIGURE 12. Enthalpy profile with downdraft: (*a*) ambient profile for case (3); (*b*) profile with $\overline{w} = -0{\cdot}1$.

Since the model formulated for the radiative heat sink is somewhat arbitrary, it is worthwhile to show that the results do not depend on the model chosen. Accordingly, case (3) is repeated for a non-linear model, in which (6.10) takes the form

$$R'' = -f(z)\,\eta^2, \tag{6.19}$$

with f given by

$$f(z) = \eta_{azz}/\eta_a^2. \tag{6.20}$$

The results (figure 13) are unchanged from those of the linear model (figure 12); the choice of radiative models, at least within this simple framework, makes little difference.

It is the sense of these results that, whatever model is chosen to represent the ambient process of the late summer tropical atmosphere, the energy profile that these processes support is, in the downdraft region, only marginally affected

by the swirling flow and the resultant boundary-layer flows of the hurricane. The primary effect of the wind fields is the slight depression of the profile by the downdraft and the very small increase in the flux at the sea surface. There is, therefore, no significant 'oceanic heating' in the sense of substantial *additional* sensible heat and water vapour transfer due to the wind fields; instead the boundary-layer energetics of the hurricane are dominated by the ambient vertical energy balance (the upward transfer of sensible and latent heat by turbulent mixing and cumulus convection and the radiative cooling) of the tropical atmosphere. Hence the use of thermodynamics based on ambient conditions for the

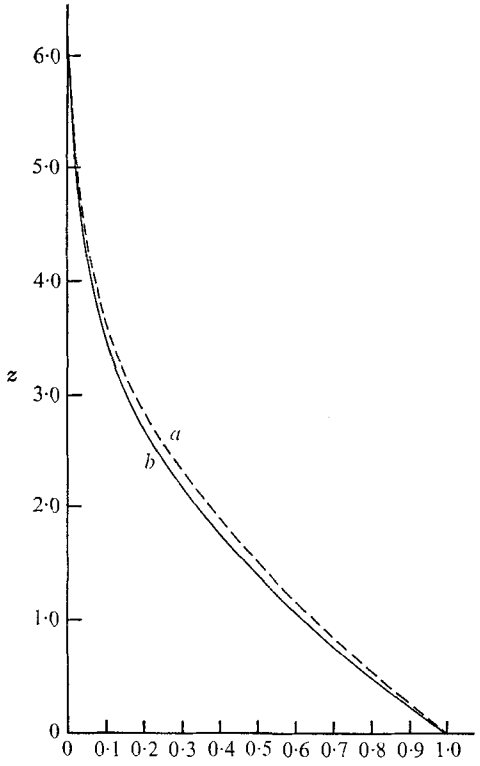

FIGURE 13. Enthalpy profile with downdraft: non-linear radiative model: (*a*) ambient profile for case (3); (*b*) profile with $\overline{w} = -0{\cdot}1$.

maximum velocity estimates in § 4 is consistent with these results. The energy supply for the storm does not, in this view, depend upon augmentation from the sea surface in the boundary layer, but rather on the heat and moisture content of the mid-troposphere air of the swirl region (and the ambient processes which maintain the ambient profile).

7. Discussion

The implications of the foregoing sections can be noted concisely.

Since the region which contains high angular momentum fluid is a few miles deep and since the downdraft in a large storm ($r_0 = O$[1000 miles]) is of the order

of 1/200 miles per hour, a hurricane could last 30 days or more before it used up its angular momentum provided only that it remained over warm enough water so that the analysis of § 6 is appropriate.

The replacement of moisture, which is characteristic of the phenomenon in oceanic locations, cannot continue over land. Thus, as the downdraft into the boundary layer continues to supply air for the updraft, that air contains less and less enthalpy as time goes on. Accordingly, the updraft column becomes heavier as its incoming enthalpy supply is depleted in a very few days and the over-land duration of an intense storm is, at most, a few days.

The intensity (wind speed) which can be achieved when the foregoing idealized configuration draws on the very simple dynamic and thermodynamic processes is significantly greater than any speeds which have actually been observed or inferred in real storms. It is clear that, even when one takes into account the inevitable 'losses' in the system and the departure from ideality (especially in the eye) no additional subtler mechanisms or processes need to be invoked to render the model consistent. The mechanisms we have described already provide all that is needed to maintain such configurations.

Parts of this study were supported by the National Science Foundation under Contract NSF-GP-17383, by the Office of Naval Research under Contract Nooo14-67-A-0298-0002, and by TRW Independent Research and Development Program.

REFERENCES

ANDERSON, O. L. 1966 Numerical solutions of the compressible boundary-layer equations for rotating axisymmetric flows. Ph.D. thesis in Aeronautical Eng'g, Hartford Graduate Center of the Rensselaer Polytechnic Institute of Connecticut.

CHARNEY, J. & ELIASSEN, A. 1964 On the growth of the hurricane depression. *J. Atmos. Sci.* **21**, 6875.

GEORGE, O. D. 1970 The boundary-layer dynamics under swirling flows in a rotating system. Ph.D. Thesis, Harvard University.

GOLDSTEIN, S. 1960 *Lectures on Fluid Mechanics*. Cambridge University Press.

HAMMOND, A. L. 1970 Boundary layer energy transfer under swirling flows: Hurricane energetics. Ph.D. Thesis, Harvard University.

LANCE, G. N. & ROGERS, M. H. 1960 The rotationally symmetric flow of a viscous fluid in the presence of an infinite rotating disk. *J. Fluid Mech.* **7**, 617–631.

JORDAN, C. L. 1957 A mean atmosphere for the West Indies Area. *National Hurricane Research Project Report*, no. 6, U.S. Department of Commerce, Washington, D.C.

MALKUS, J. 1962 Large scale interactions. In *The Sea*, vol. 1 (ed. M. N. Hill), pp. 88–294. Interscience.

MALKUS, J. & RIEHL, H. 1960 On the dynamics and energy transformations in steady-state hurricanes. *Tellus*, **12**, 1–20.

OOYAMA, K. 1969 Numerical simulation of the life cycle of tropical cyclones. *J. Atmos. Sci.* **26**, 3–40.

PRIESTLEY, C. H. B. 1959 *Turbulent Transfer in the Lower Atmosphere*. University of Chicago Press.

ROSENBERG, S. 1969 Numerical experiments with a multilevel primitive equation model designed to simulate the development of tropical cyclones. *ESSA Technical Memorandum* ERLTM-NHRL 82, Nat'l Hurricane Research Laboratory. Miami.

SMITH, R. K. 1968 The surface boundary layer of a hurricane. *Tellus*, **20**, 473–484.

YAMASAKI, M. 1968 A tropical cyclone model with parameterized vertical partition of released latent heat. *J. Meteor. Soc. Japan*, Series II, **46**, 202–214.